JOURNAL OF GUIDANCE, CONTROL, AND DYNAMICS
Vol. 21, No. 3, May–June 1998

Dynamics of an Asymmetric Gyrostat

A. C. Or*
University of California, Los Angeles, Los Angeles, California 90024-1567

The nonlinear despin dynamics of a gyrostat with a symmetric balanced platform and an asymmetric rotor (can be balanced or unbalanced) is studied. A numerical scheme is provided for computing the multiple equilibria as well as their bifurcation properties. The major purpose is to determine the boundary curves between normal-spin and flat-spin transitions in terms of motor torque magnitude and initial conditions, rotor asymmetry, and imbalance, when the torque is not considered small. Results show alternating regions of normal- and flat-spin states in the range of torque magnitude.

I. Introduction

A GYROSTAT has long been used as a dynamical model for older generations of artificial satellites.[1,2] Despite the numerous studies that have been done on gyrostatic dynamics in the past,[3–14] few address the nonlinear aspects of the motions, and some of the anomalous characteristics of the motions remain unclear largely due to the nonlinearity of motions. Although dual-spin dynamics becomes less important in satellite designs, the complex properties of motions may still be of interest to dynamicists in general and deserve a closer look.

Early on, two types of settling states of a despin maneuver were studied through computer simulations.[3,6–8] One type is called normal-spin transition, when the settling motion accompanied by nutation does not change the spin orientation relative to the body's axes. The other type is called flat-spin or anomalous transition because there are changes in spin orientation. Surprisingly, long before aerospace engineers identified the anomalous behavior[3] associated with spacecraft maneuver, Masaitis[14] studied the nonlinear motions of a force-free gyrostat and reported the existence of multiple equilibria. Masaitis also reported their stability and bifurcation characteristics as a function of the relative speed between the two bodies. Rand et al.[11] considered a simpler generic mechanical model to explain the nonlinear transitional behavior. The authors coined the term *resonance capture* in contrast to the term *trap* used by some other authors in association with the flat-spin transition. Using a dual-spin gyrostat model, Hall and Rand[12] studied the forced nonlinear motions for a small motor torque. The small-torque results show that the forced motions remain close to a stable branch of the equilibrium curve. When the asymmetry is large, a flat-spin branch can replace the normal-spin branch as the stable solution. In other words, it becomes a trap state. More recently, Tsui and Hall[13] developed a probabilistic approach to the capture problem when motor torque magnitude is no longer assumed small.

In this paper we provide a numerical scheme for computing multiple equilibrium solutions and determining their stability and bifurcation properties simultaneously for equations that do not necessarily possess a potential. Another purpose is to reexamine the forced nonlinear motions of a gyrostat and determine the boundary curves of the two different spin transitions in terms of the motor-torque magnitude, initial body angular rates, rotor asymmetry, and imbalance. So far, the boundaries for different types of transitions have not been determined when the motor torque is not small.

II. Variational Scheme for Computing Multiple Equilibria

Consider the motion of a gyroscopic body. In the absence of external forces, Euler's equation for the body in vector form is

$$\dot{\boldsymbol{h}} = -\boldsymbol{\omega} \times \boldsymbol{h} \tag{1}$$

The equilibria are given by

$$\boldsymbol{\omega} \times \boldsymbol{h} = \boldsymbol{0} \tag{2}$$

The trivial solution is $\boldsymbol{\omega} = \boldsymbol{0}$. For nontrivial solutions, $\boldsymbol{\omega}$ and $\boldsymbol{h}$ are parallel vectors. Two constants of motions can be formed from Eq. (1): 1) by taking the dot product of Eq. (1) with $\boldsymbol{\omega}$ and 2) by taking the dot product with $\boldsymbol{h}$. The first operation gives the kinetic energy E. The second gives the square of total angular momentum. The following scheme is a variation of those in elementary catastrophe theory.[15]

The scheme is applicable to more general problems, but the simple example given here is a gyrostat with a symmetric and balanced platform $\mathcal{P}$ and an asymmetric unbalanced rotor $\mathcal{R}$. Both bodies' centers of mass are located on their common geometric axis. The two bodies are hinged on a bearing unit so that they can rotate freely about a common axis. For a sketch of the gyrostat, readers are referred to earlier papers, e.g., by the author.[10]

The total angular momentum of the gyrostat, $\boldsymbol{h}$, is given by

$$\boldsymbol{h} = \boldsymbol{I}\boldsymbol{\omega} + \boldsymbol{h}_p \tag{3}$$

where $\boldsymbol{I}$ is the moment of inertia tensor of the dual-spin system not including the axial moment of inertia of the platform,

$$\boldsymbol{I} = \begin{pmatrix} I_1 & 0 & I_{13} \\ 0 & I_2 & I_{23} \\ I_{13} & I_{23} & I_3 \end{pmatrix} \tag{4}$$

where I_p is the axial moment of inertia of the platform, and $\boldsymbol{\omega} = (\omega_1, \omega_2, \omega_3)'$ and $\boldsymbol{h}_p = (0, 0, I_p\omega_p)'$, both column vectors. Subscript p denotes the platform; $\boldsymbol{x}'$ denotes the transpose of $\boldsymbol{x}$. The energy functional E is defined by

$$E = \tfrac{1}{2}\left(\boldsymbol{\omega}'\boldsymbol{I}\boldsymbol{\omega} + I_p\omega_p^2\right) \tag{5}$$

For angular momentum the expression of h^2 is

$$h^2 = (\boldsymbol{I}\boldsymbol{\omega} + \boldsymbol{h}_p)'(\boldsymbol{I}\boldsymbol{\omega} + \boldsymbol{h}_p) \tag{6}$$

In a despin maneuver, the value of h^2 is given by the initial conditions. For stability analysis, it is convenient to introduce a Lagrangian function L,

$$L(\boldsymbol{\omega}) = E(\boldsymbol{\omega}) + \lambda\left[h^2 - (\boldsymbol{I}\boldsymbol{\omega} + \boldsymbol{h}_p)'(\boldsymbol{I}\boldsymbol{\omega} + \boldsymbol{h}_p)\right] \tag{7}$$

where λ is the Lagrange multiplier. We can now Taylor-expand L in the neighborhood of an equilibrium to obtain an approximation of L up to the second-order terms:

$$L = L_s + [\boldsymbol{\omega}_s'\boldsymbol{I} - \lambda(\boldsymbol{I}\boldsymbol{\omega}_s + \boldsymbol{h}_p)'\boldsymbol{I}]\delta\boldsymbol{\omega} + \tfrac{1}{2}\delta\boldsymbol{\omega}'(\boldsymbol{I} - \lambda\boldsymbol{I}^2)\delta\boldsymbol{\omega} + \cdots \tag{8}$$

where s denotes steady state. Equilibria are obtained from Eq. (8) by requiring the first-order term multiplied to $\delta\boldsymbol{\omega}$ to vanish. This provides three equations for three components of $\boldsymbol{\omega}$ and λ. The

Received July 18, 1996; revision received Nov. 12, 1997; accepted for publication Nov. 12, 1997.

*Research Associate, Department of Mechanical and Aerospace Engineering.

fourth equation is the constraint relationship (6). The problem can be readily solved by an iterative approach.

In the stability analysis, an order reduction of the second-order quadratic term is required, because the perturbations near an equilibrium are no longer arbitrary because of the angular momentum constraint. Applying Eq. (6) to the second-order problem, we obtain in differential form

$$(\boldsymbol{I}\boldsymbol{\omega}_s + \boldsymbol{h}_p)'\boldsymbol{I}\delta\boldsymbol{\omega} + \delta\boldsymbol{\omega}'\boldsymbol{I}^2\delta\boldsymbol{\omega} + \cdots = 0 \tag{9}$$

For order reduction we write the first-order term of Eq. (9) as $\boldsymbol{c}'\delta\boldsymbol{\omega} = 0$, where the three components c_i are functions of the steady-state variables. If the axial angular momentum is nonvanishing so that $c_3 \neq 0$, then we can eliminate $\delta\omega_3$. We write

$$\delta\omega_3 = -(1/c_3)\tilde{\boldsymbol{c}}'\delta\tilde{\boldsymbol{\omega}}$$

where $\boldsymbol{c}$ and $\boldsymbol{\omega}$ are partitioned so that $\boldsymbol{c} = (\tilde{\boldsymbol{c}}, c_3)'$ and $\boldsymbol{\omega} = (\tilde{\boldsymbol{\omega}}, \omega_3)'$. The following matrix is also partitioned according to

$$\boldsymbol{I} - \lambda\boldsymbol{I}^2 = \begin{pmatrix} \tilde{\boldsymbol{I}}_1 & \tilde{\boldsymbol{I}}_2 \\ \tilde{\boldsymbol{I}}_2' & I_3 \end{pmatrix} \tag{10}$$

With some algebraic manipulations, we obtain a reduced second-order term $\frac{1}{2}\delta\tilde{\boldsymbol{\omega}}'\boldsymbol{H}\delta\tilde{\boldsymbol{\omega}}$, where the Hessian $\boldsymbol{H}$ is given by

$$\boldsymbol{H} = \left[\tilde{\boldsymbol{I}}_1 - (2/c_3)\tilde{\boldsymbol{I}}_2\tilde{\boldsymbol{c}}' + \left(I_3/c_3^2\right)\tilde{\boldsymbol{c}}\tilde{\boldsymbol{c}}'\right] \tag{11}$$

The bifurcation corresponds to the vanishing condition of the determinant of $\boldsymbol{H}$. Such a condition can be built into the iterative scheme, which is now used to compute the equilibria and the singularities simultaneously.

III. Euler's Equations for Numerical Integration

To determine the transition curves, Eq. (1) is integrated in time for given initial conditions. In a component form, the Euler equations for a gyrostat with a symmetric and balanced platform and an asymmetric and dynamically unbalanced rotor are

$$I_1\dot{\omega}_1 + (H_3 - I_2\omega_3)\omega_2 = -I_{13}\omega_1\omega_2 - I_{13}\dot{\omega}_3 \tag{12a}$$

$$I_2\dot{\omega}_2 - (H_3 - I_1\omega_3)\omega_1 = -I_{13}\left(\omega_3^2 - \omega_1^2\right) \tag{12b}$$

$$I_3\dot{\omega}_3 + (I_2 - I_1)\omega_1\omega_2 = -I_{13}\dot{\omega}_1 + I_{13}\omega_2\omega_3 + T_m \tag{12c}$$

$$I_p\dot{\omega}_p = -T_m \tag{12d}$$

where $H_3 = I_3\omega_3 + I_p\omega_p$ is the total axial component of angular momentum, T_m is an axial motor torque, and ω_1, ω_2, ω_3, and ω_p are the two transverse rates and the axial rates of $\mathcal{R}$ and $\mathcal{P}$, both measured in the common body frame. For simplicity it is assumed that in Eqs. (12) the rotor has only one component of imbalance, i.e., $I_{12} = I_{23} = 0$. The variational scheme of Sec. II also allows $I_{23} \neq 0$. Throughout the study we assume $I_1 > I_2 > I_3 > I_p$. In the subsequent numerical solutions, the equations of motion and their parameters and dependent variables are assumed to be nondimensional. The dimensional moments of inertia components are scaled by I_3, and the dimensional angular rates by $\omega_3(0)$. Time is scaled by $\omega_3(0)$. The motor torque T_m is scaled by $I_3\omega_3^2(0)$. At $t = 0$, the initial conditions are $\omega_3(0)$ and $\omega_p(0) = 1$.

For a symmetric balanced platform, ω_p can be solved explicitly as a function of time from the last equation. The forcing T_m is assumed constant. We integrate the equations in time using a fourth-order Runge–Kutta method. We examine the transitional behavior from the time series. A time step size of 0.01–0.02 gives sufficient accuracy.

IV. Results

A. Multiple Equilibria and Stability

For the cases we choose to study, the parameters are $I_1 = 1.5$, $I_2 = 1.2$, $I_3 = 1.0$, $I_p = 0.7$, and $I_{12} = 0$. The axial initial conditions are $\omega_3 = \omega_p = 1$ at time zero. For the case of a completely balanced rotor, two pitchfork bifurcations occur at 1) $\omega_p = (I_1 - I_3)h/I_1I_p$ and 2) $\omega_p = (I_2 - I_3)h/I_2I_p$. In Fig. 1, the first bifurcation is shown as point B and the second bifurcation as point C on the equilibrium curves showing the kinetic energy E. At point A of the despin maneuver ($t = 0$), an internal axial moment is turned on at the hinge of the gyrostat. The moment forces ω_p to decrease linearly in time. At $\omega_p = 0$, the despin is completed and the motor torque is turned off. Because $I_1 > I_2$, bifurcation point 1 occurs first (point B) and gives rise to a new pair of equilibria. This pair of equilibria are stable and have identical energy. They are shown by a solid curve emerging from point B and extending to the left region. The new equilibria have a spin orientation directed along a pair of tilted axes that are symmetrical about the geometric axis. The normal-spin equilibrium becomes a saddle point (dashed line) after passing to the left of point B. The normal-spin equilibrium regains stability after passing to the left of point C. At point C, a second pitchfork bifurcation occurs giving rise to another two new equilibria. But in this case both new solutions are unstable. The two bifurcation points divide the despin range of ω_p into three regions, according to their number of equilibria. Two equilibria exist to the right of point B. Both are normal-spin states; one corresponds to corotating and the other to counter-rotating bodies. Between points B and C, there are four equilibria. To the left of point C, there are six equilibria. The counter-rotating normal-spin equilibrium is stable in the despin range. The three regions from right to left, therefore, have two, three, and four stable equilibria, respectively.

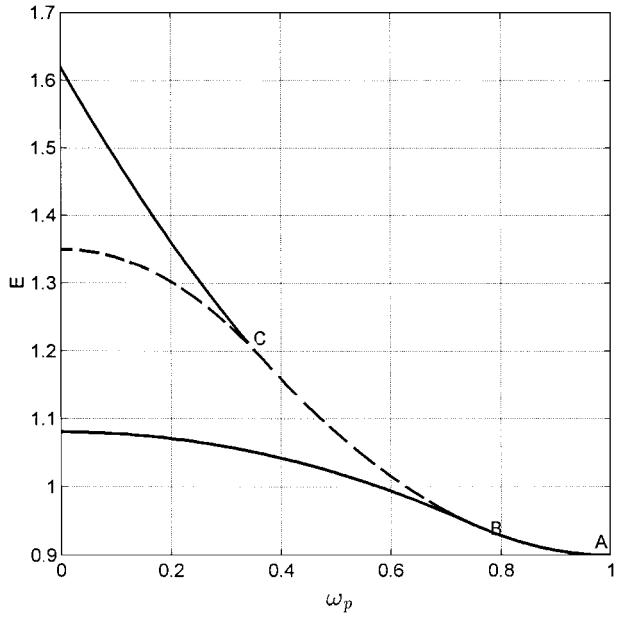

Fig. 1 Energy curves showing the multiple equilibria and bifurcation points in the despin range of ω_p.

The two products of inertia I_{13} and I_{23} are unfolding parameters of the pitchfork bifurcations. Next, we consider both products of inertia to be nonzero and show the angular rates of the multiple equilibria in the despin range including the distortion arising from the dynamic imbalances. In Figs. 2a and 2b, we let $I_{13} = I_{23} = 0.02$ and show the equilibrium curves of the two transverse rates ω_i $(i = 1, 2)$ of all six solutions. In Fig. 2, the choice of line types does not have any implication on the stability property. The normal counterspin curve is shown as the dotted line. The transverse rates are small for this solution. Figure 2a corresponds to an imperfect pitchfork bifurcation (corresponding to point B of Fig. 1) in ω_1. In an imperfect situation, the normal-spin curve is connected with one of the pitchforks to become a continuous branch. The unstable normal-spin curve is shown as the dashed-dotted line, which connects with a second stable branch of pitchfork via a fold. The inset in Fig. 2a gives a magnified view near the second bifurcation, which is not clearly displayed in the main figure due to the fine resolution. Similarly, Fig. 2b shows the second imperfect pitchfork bifurcation (compared with point C of Fig. 1) in ω_2. The Fig. 2b inset provides a magnified view near the first bifurcation.

In a parameter plane consisting of the control parameter ω_p and the unfolding parameter, either I_{13} or I_{23} (depending on whether

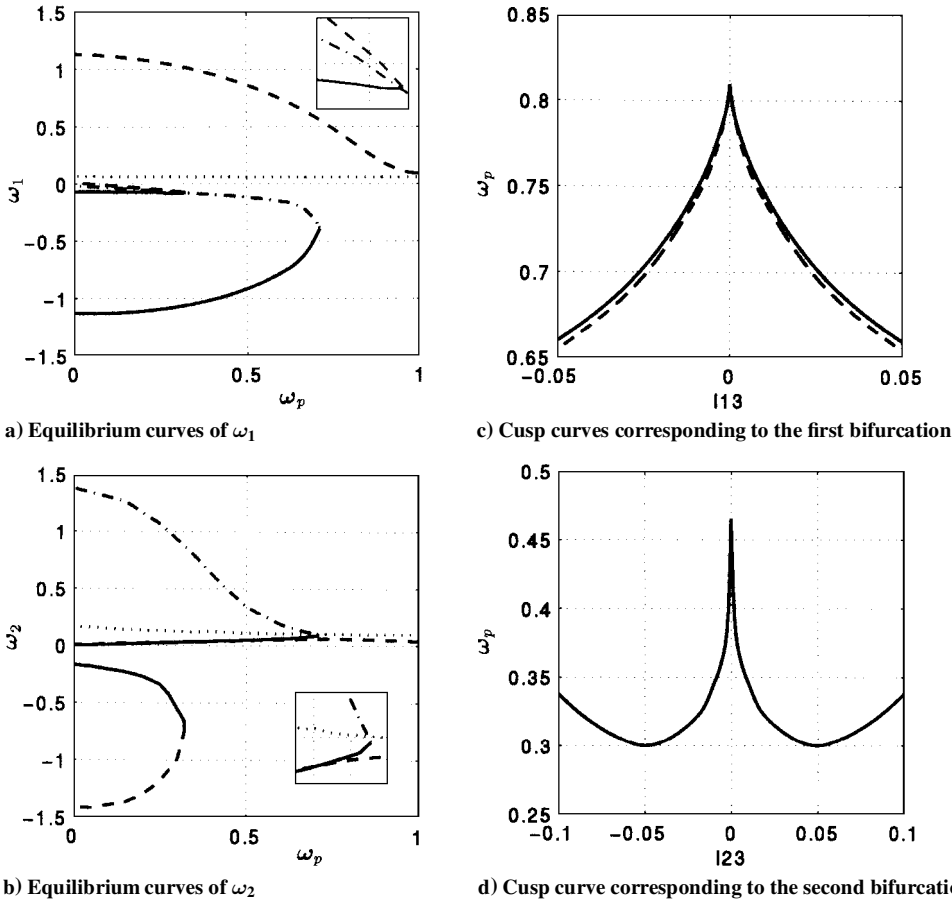

Fig. 2 Equilibrium curves in the despin range of ω_p showing the imperfect pitchfork bifurcations and cusp curves with I_{13} as the unfolding parameter.

it is the first or second bifurcation), we can show the cusp structure. Such a structure is one of seven types of singularities possible on a two-dimensional parameter plane according to the catastrophe theory.[15] The unfolding parameter of the first cusp point is I_{13}. Figure 2c shows that the first cusp is symmetrical about the vertical. Its tip occurs at about $\omega_p = 0.8056$. This corresponds to the bifurcation point B of Fig. 1. The solid (dashed) line corresponds to $I_{23} = 0$ ($I_{23} = 0.02$). The cusp is two dimensional. For the same value of ω_p, there is no cusp structure in the I_{23}–ω_p section. A pair of cusp curves delimits two distinct regions in terms of solution characteristics. There are two solutions above the cusp curves and four solutions below them. A similar cusp structure corresponding to the second bifurcation in the unfolding parameter I_{23} is shown in Fig. 2d.

B. Transitions Between Different Spin States

In Fig. 3, we show two trajectories of motions that start with the same initial conditions but correspond to slightly different values of T_m and then end up in different states of spin orientation after the despin. The trajectories are shown in a three-dimensional phase portrait. The initial conditions are $\omega_3 = \omega_p = 1$, $\omega_1 = 0$, and $\omega_2 = 0.3$. The bodies are balanced, i.e., $I_{13} = I_{23} = 0$. In Fig. 3, the normal transition (solid line) corresponds to the smaller torque value, at $T_m = 10.05 \times 10^{-3}$. The anomalous transition (dashed line) corresponds to the slightly larger torque value at $T_m = 10.1 \times 10^{-3}$. The solid trajectory is called normal because the final orbit's spin orientation is the same as the initial spin orientation. In this case, the rotor is spun up. The dashed trajectory is anomalous because the final orbit's spin orientation becomes oblique. Even though the total angular momentum vector remains fixed in space, the body's orientation changes as indicated by the spin down of the rotor. Because the transverse angular momentum component is significantly increased, this anomalous state is sometimes called flat spin. In the time history, ω_p reaches zero at about $t = 67$. For $t > 67$ we set T_m to zero. But the two trajectories start to diverge from one another right after $t = 25$. The turning off of T_m at the end of despin will stop energy from pumping into the motions but has no effects on the switch over between the two types of transitions. In an earlier study by Tsui and Hall,[13] the authors used a probabilistic approach they borrowed from celestial mechanics to determine the transitions between two types of end motions. It is important to recognize, however, for a deterministic system, there is a well-defined boundary surface in the parameter and initial phase spaces separating the two types of end motions. Such a boundary surface can be determined numerically.

In Figs. 4a–4d, we determine the dependence of this boundary on 1) initial condition of transverse angular rates, 2) rotor asymmetry, 3) rotor imbalance, and 4) initial axial angular momentum. In the results of Fig. 4 it is assumed that T_m is constant in the range $0 < \omega_p \leq 1$ but zero outside this range. The initial conditions on axial spin speeds are $\omega_3 = \omega_p = 1$. In Fig. 4a, $h^2 = 3.02$ and remains constant. The imbalances are zero, i.e., $I_{13} = I_{23} = 0$. Figure 4a shows that the threshold curve is made up of three connected segments. This curve divides the ω_1–T_m plane into three main regions. There is a narrow strip region between the lower and middle regions. The lower region corresponds to a flat-spin transition; the strip region corresponds to normal-spin transition; the middle region corresponds to flat-spin transition again; and finally, the upper region corresponds to normal-spin transition. The range of ω_1 shown in Fig. 4 is from -0.24 to 0.24. The existence of the intermediate boundaries appears to have evaded previous investigations. Because normal-spin transition can occur within the strip region at a moderately small T_m, it may provide an optimal window for despin maneuver from the applicational point of view of spacecraft.

Next, we turn to the dependence of the boundary surface on the asymmetry of rotor. We let I_1, I_3, and I_p be constant and vary I_2. The initial conditions are such that $\omega_1 = 0$ and $\omega_3 = \omega_p = 1$. To keep the angular momentum constant, at $h^2 = 3.02$, we vary ω_2 in the initial condition according to

$$\omega_2(0) = \left[h^2 - (I_3 + I_p)^2 - \omega_1(0)^2\right]^{\frac{1}{2}}$$

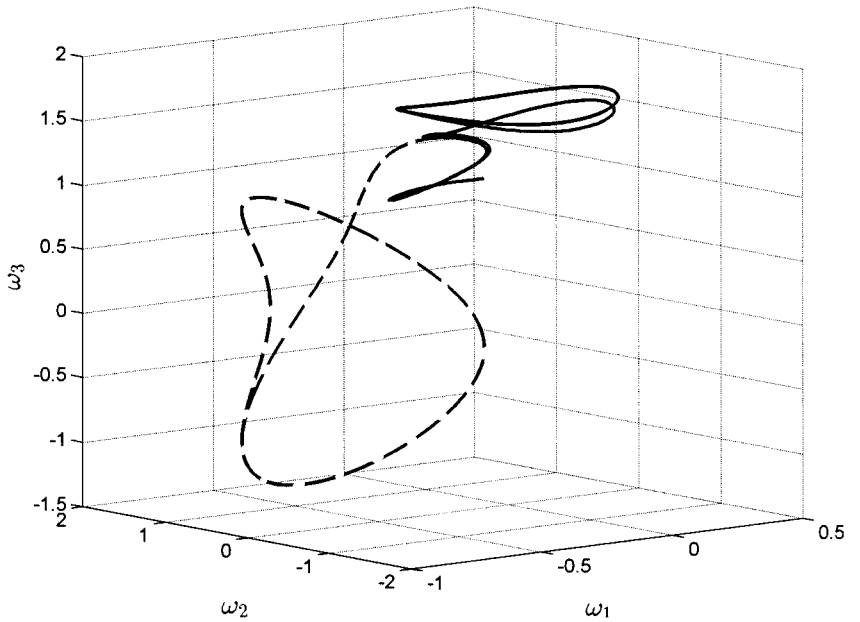

Fig. 3 Pair of phase-space trajectories showing the normal-spin and flat-spin transitions.

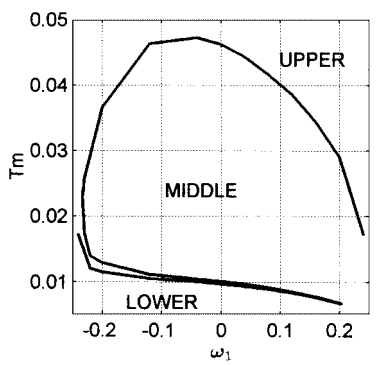

a) T_m **vs initial transverse rate** ω_1

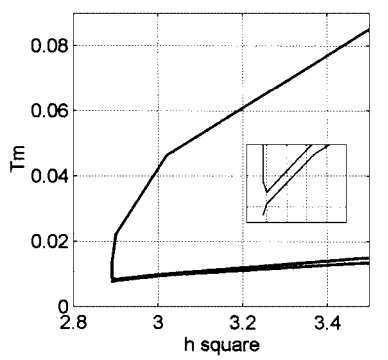

c) T_m **vs** h^2

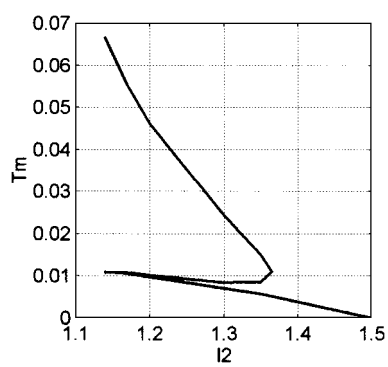

b) T_m **vs** I_2

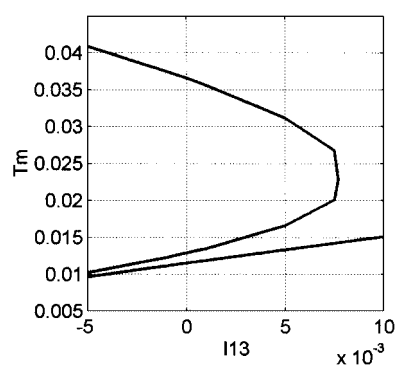

d) T_m **vs** I_{13}

Fig. 4 Boundary curve between the two-regime transitions.

Again, we assume a balanced rotor. The asymmetry can be measured by the quantity $2(I_1 - I_2)/(I_1 + I_2)$. In Fig. 4b, as asymmetry decreases by increasing I_2 toward I_1, we see that the middle flat-spin region disappears at about $I_2 = 1.37$. To the left, the strip region also disappears near $I_2 = 1.14$ when the asymmetry is large. Therefore, asymmetry is seen to promote flat-spin motions.

We now turn to the dependence on angular momentum level. Let $I_2 = 1.2$, $\omega_1 = 0$, $\omega_3 = \omega_p = 1$ at $t = 0$, and let h vary. The value of ω_2 again is determined from the value of h^2. Again, the products of inertia are set to zero. Figure 4c shows how the threshold curve depends on h^2. As h^2 increases, the gyrostat naturally requires a larger torque to have a successful despin. The strip region also widens as h^2 increases. To the left, when h^2 approaches value 2.89, the initial transverse rates become very small. At this angular momentum level, a normal transition seems possible for all T_m. In the magnified view included in Fig. 4c, as the strip region comes to its end both curves show sharp turns as the transverse rates tend to zero.

So far in Figs. 4a–4c, the rotor is assumed perfectly balanced. Including a small product of inertia may make the result more realistic. Effects of large imbalance were studied by Tsui and Hall[13] and will not be discussed here. Here, we assume I_{13} is nonvanishing but $I_{23} = 0$. The moments of inertia are the same as before: $I_1 = 1.5$, $I_2 = 1.2$, $I_3 = 1$, and $I_p = 0.7$. Contrary to the common notion, a small imbalance can actually promote normal-spin transition if I_{13} has the right sign. We consider the case with $h^2 = 3.02$, with $\omega_1 = -0.2$ at $t = 0$. Figure 4d shows that the middle flat-spin region disappears if I_{13} is larger than about 7.6×10^{-3}.

V. Concluding Remarks

For a small forcing, the stability behavior of a gyrostat in a despin maneuver can be described adequately by a quasistatic or time-averaging approach. In this case, the motions can be viewed as slightly perturbed about a stable equilibrium solution. In terms of the stability dependence of parameters, a diagram showing the equilibria, such as Fig. 1, seems adequate.

On the other hand, when the motor torque is not small the despin motions can be more complicated. For a given set of parameters and angular-rate initial conditions, the despin will either preserve the initial spin orientation relative to the body or will promote a transition into the flat-spin trap.

Our numerical results indicate that, if T_m is sufficiently large, a normal-spin transition will occur. If T_m is sufficiently small, a flat-spin transition will result. More surprisingly, besides the upper normal-spin and the lower flat-spin regions, there exist two more regions in between: a narrow strip region in which a normal-spin transition can occur and a middle region above it corresponding to a flat-spin transition. The existence of these two intermediate regions seems to have evaded previous attention. If despin is designed to minimize fuel consumption, then the strip region can serve as an optimal window for the maneuver.

Acknowledgment

The author is grateful to the California Space Institute for its support of this work.

References

[1]Hughes, P. C., *Spacecraft Attitude Dynamics*, Wiley, New York, 1986.

[2]Wertz, J. R. (ed.), *Spacecraft Attitude Determination and Control*, D. Reidel, Boston, 1984.

[3]Scher, M. P., and Farrenkopf, R. L., "Dynamic Trap States of Dual Spin Spacecraft," *AIAA Journal*, Vol. 12, 1974, pp. 1721–1725.

[4]Cochran, J. E., "Nonlinear Resonances in the Attitude Motion of Dual-Spin Spacecraft," *Journal of Spacecraft and Rockets*, Vol. 14, 1977, pp. 562–572.

[5]Cochran, J. E., and Beaty, J. R., "Near-Resonant and Transition Attitude Motion of a Class of Dual-Spin Spacecraft," *Journal of the Astronautical Sciences*, Vol. 26, 1978, pp. 19–45.

[6]Tsuchiya, K., "Attitude Behavior of a Dual-Spin Spacecraft Composed of Asymmetric Bodies," *Journal of Guidance and Control*, Vol. 2, 1979, pp. 328–333.

[7]Adams, G. J., "Dual-Spin Spacecraft Dynamics During Platform Spinup," *Journal of Guidance and Control*, Vol. 3, 1980, pp. 29–36.

[8]Hollars, M. G., "Minimum Energy Trap States of Dual-Spin Spacecraft," *Journal of Guidance, Control, and Dynamics*, Vol. 5, 1982, pp. 286–290.

[9]Lebsock, K. L., "Despin Through Unity Inertia Ratio," *Journal of the Astronautical Sciences,* Vol. 30, 1982, pp. 213–227.

[10]Or, A. C., "Resonances in the Despin Dynamics of Dual-Spin Spacecraft," *Journal of Guidance, Control, and Dynamics*, Vol. 14, 1991, pp. 321–329.

[11]Rand, R. H., Kinsey, R. J., and Mingori, D. L., "Dynamics of Spinup Through Resonance," *International Journal of Nonlinear Mechanics*, Vol. 27, 1992, pp. 489–502.

[12]Hall, C. D., and Rand, R. H., "Spinup Dynamics of Axial Dual-Spin Spacecraft," *Journal of Guidance, Control, and Dynamics*, Vol. 17, 1994, pp. 30–37.

[13]Tsui, R., and Hall, C. D., "Resonance Capture in Unbalanced Dual-Spin Spacecraft," *Journal of Guidance, Control, and Dynamics*, Vol. 18, 1995, pp. 1329–1335.

[14]Masaitis, C., "On the Motion of Two Linked Bodies," *Archive for Rational Mechanics and Analysis*, Vol. 8, 1961, pp. 23–35.

[15]Hilton, P. J. (ed.), *Structural Stability, the Theory of Catastrophes and Applications in the Sciences,* Springer-Verlag, Berlin, 1976.